Study of high energy (25-10000 GeV) interactions with a multiplate cloud chamber using Monte Carlo simulations for energy calibration

1972 J. Phys. A: Gen. Phys. 5 859

(http://iopscience.iop.org/0022-3689/5/6/011)

J. Phys. A: Gen. Phys., Vol. 5, June 1972. Printed in Great Britain

Study of high energy (25–10 000 GeV) interactions with a multiplate cloud chamber using Monte Carlo simulations for energy calibration

R H VATCHA, B V SREEKANTAN and S C TONWAR

Tata Institute of Fundamental Research, Bombay-5, India

MS received 16 December 1971

Abstract. Monte Carlo simulations of hadron and electron–photon cascades in the large multiplate cloud chamber operating at Ootacamund (India) have been carried out using some plausible interaction models. Some extreme assumptions about multiplicity and inelasticity have been incorporated in order to study their effect on the detailed features of the cascades. A new method for estimating the energies of the cascades of energy above about 200 GeV by measuring 'cascade widths' at different depths in the absorber has been developed with calibrations provided by the simulations. The estimated energy is accurate to within 50%. The experimentally observed cascades due to pions and nucleons at energies below 200 GeV are similar and a comparison of the detailed profiles with the simulated cascades suggests that pions like nucleons are only partially inelastic at these energies. Hadron cascades in the TeV energy range show rather fast absorption after the cascade maxima. This feature suggests the possibility of an increase in inelasticity and multiplicity, or an increase in the fraction of energy transferred to the soft component in TeV collisions of hadrons with iron nuclei, compared to these characteristics at lower energies.

1. Introduction

A large multiplate cloud chamber has been operated in association with the TIFR air shower array at Ootacamund to study the properties of the high energy hadronic component in showers of size 5×10^4 to 5×10^6 particles. During this study it has been possible to elucidate several features of the high energy interactions of hadrons in the energy range 25–10 000 GeV. Since the cloud chamber has, in the form of 21 iron plates, 21 radiation lengths of absorber and about 2·2 interaction mean free paths for collisions of hadrons, it has been feasible to use the integral track length method for the evaluation of the energy of the hadrons. In the case of hadron cascades of energy above about 200 GeV the track density becomes so high close to the cascade axis especially in the regions near the maxima that in the corresponding cloud chamber photographs saturation effects set in and it becomes impossible to count individual tracks. In order to obtain the track lengths in such cases we have developed a new method which depends upon the measurement of 'cascade widths' at different stages of the cascades and have successfully used this method for the determination of hadron energies up to tens of TeV. Monte Carlo simulations of the hadron–electromagnetic cascades in the plates of the chamber are used to obtain the relation between the primary hadron energy and the track lengths corresponding to different stages of development and absorption of the cascades. The same calculations are further elaborated to obtain the relation between the projected cascade widths at different stages and the corresponding number of tracks. This enables

the determination of the track length to be made whenever a track count is not directly possible. Since in the present method the developments of both the hadronic cascade and the secondary electromagnetic cascade through the plates of the chamber are taken into account, the primary hadron energy is more accurately determined than in those methods in which the track length is related to the development of the pure electromagnetic cascade resulting from the gamma rays (the decay products of π^0 mesons) which are produced only in the first collision of the hadrons. In the latter method the hadron energy is estimated by multiplying the electromagnetic cascade energy by a factor of six on the basis that the inelasticity in the first collision is 0·5 and the fraction going in the π^0 mesons is a third of the total inelasticity. This method which has been used in many of the earlier investigations leads to systematic overestimates of the energy even if one uses a plate assembly of lead in which the ratio of the radiation length to the interaction mean free path is approximately 30. At high energies because of the high secondary multiplicity the contribution to the cascade from the second and higher generation collisions is quite appreciable. From our calculations we find that at about 100 GeV the energy is overestimated by a factor greater than about 2, and the fluctuations in the fraction of energy transferred to the π^0 component in the first collision only, lead to considerable uncertainty in energy estimates.

In this paper, we present the details of the new method for the evaluation of the energy of the cascades in the energy range 25–10 000 GeV and present some of the results on the characteristics of high energy interactions of pions and nucleons that have been obtained from a comparison of the detailed profiles of the experimentally obtained cascade curves with Monte Carlo simulations which are based on a few different models of hadron interactions.

2. Monte Carlo simulation of hadron and electron–photon cascades in the cloud chamber plate assembly

2.1. Simulation procedure

The hadron and electron–photon cascades have been simulated for the particular configuration of the plate assembly in the cloud chamber in operation with the TIFR air shower array at Ootacamund (800 g cm^{-2}). The chamber is made of cast iron (1 inch thick) and has dimensions of 2 m (breadth) × 1·5 m (height) × 1 m (depth). It contains 21 iron plates each having an area of 1·95 m × 0·95 m and thickness of 1·8 cm. These plates are separated from each other by an average distance of 2·8 cm. Thus apart from the cast iron top plate of the chamber body, there is nearly 290 g cm^{-2} of absorber inside the chamber and this is equivalent to about 2·2 interaction mean free paths for hadrons (nucleons or pions) and 21 radiation lengths (rl) for electromagnetic processes.

In the three-dimensional Monte Carlo simulations the incident hadron is required to interact in the top plate of the chamber and each particle generated in this interaction and the subsequent secondary hadronic and electromagnetic interactions is followed till it is either absorbed in the plate or it escapes from the chamber. The gaseous gaps between the iron plates are treated in the calculations as a vacuum since the amount of matter offered by the gas for any hadronic or electromagnetic interactions is negligible and the scattering in this region is insignificant except for very low energy (kinetic energy of a few MeV) electrons. However, the actual separation between the plates has to be taken into consideration since the lateral spread of the particles which is an important parameter for energy measurements depends critically on the dimensions of the gaps.

The hadron interactions are simulated using interaction models derived from available accelerator and cosmic ray data. Some of the parameters of the models have been chosen taking into account several features of the cascades observed in our chamber itself. The different models (A, B and C) incorporate variations in multiplicity, inelasticity and energy distribution among produced particles and allow us to study their effects on the observable cascade parameters such as the absolute number of particles, their lateral spread and rate of development and absorption at different stages. The lateral spread of the hadron cascades apart from the above hadron interaction properties depend on the p_t distribution in low energy hadron interactions and the multiple scattering of electrons both of which are relatively well known and are taken into account in the calculations.

The model A has assumptions about multiplicity and inelasticity such that the cascades develop slowly and also suffer attenuation relatively slowly. The assumptions made regarding the pion–iron nucleus interactions are: (i) the average effective multiplicity increases with pion energy E (GeV) as $1{\cdot}5E^{1/4}$ and (ii) the interactions are completely inelastic. The nucleon interactions are assumed to result in the formation of an isobar in most of the cases (70%) and the multiplicity in these interactions, excluding the three pions resulting from successive isobar decay, is taken as $0{\cdot}34E^{1/2}$. The average inelasticity turns out to be 0·5. Production of nucleon–antinucleon pairs is not considered since this is not expected to change significantly the cascade features in the cloud chamber. In model B isobar production is considered as in A, but the average multiplicity is assumed to be about 2·5 times higher at any energy compared to model A. This is to see the effect of higher multiplicity which should result in a more rapid development of the cascade but in this model pion interactions are considered as only partially inelastic ($\langle\eta\rangle = 0{\cdot}6$). The model C is distinct from models A and B since it assumes all the interactions to be completely inelastic and the average effective multiplicity to vary as $2{\cdot}7E^{1/4}$, slightly lower than in model B. Due to the complete inelastic nature of the interactions assumed in model C, much faster development and attenuation of the cascades is expected compared to the other models. The full details of the interaction models are discussed in Appendix 1. Fluctuations in various interaction parameters in individual interactions have been taken into account in the calculations through suitably assumed distributions. The energy going into slow particles and heavy fragments in the disintegration of iron nuclei at the sites of hadron interactions has also been considered.

The photons resulting from the decay of neutral pions generate the electron–photon cascades. The prominent features considered in the calculations for electrons and photons as they travel through the iron absorber are: multiple scattering, collision losses and bremsstrahlung radiation processes for the electrons, and pair production and Compton scattering for the photons. The multiple scattering for electrons, due to its importance in the lateral spread of the cascades, has been taken into account in a detailed manner even at the expense of increased computation time. The scattering angle is calculated for very thin strips of absorber, the thickness being as small as 5×10^{-4} rl for 1 MeV electrons. Details of the electromagnetic processes incorporated in the calculations are discussed in Appendix 2.

2.2. Results of the calculations

The following quantities are determined for each cascade generated by the computer: (i) the number of particles of different types after each absorber layer, (ii) the lateral

distribution of secondaries as projected onto a plane parallel to the cascade axis, (iii) the energy escaping after 20 rl and (iv) the energy going into the nuclear disintegrations. It has been observed from the cloud chamber photographs projected to the original dimensions of the chamber that the counting of individual tracks is feasible only at distances from the axis at which the projected track density falls below 1·5 mm^{-1}. This criterion has been used in the calculations to obtain the parameter 'cascade width' which is characteristic of the cascade after every absorber layer. The 'cascade width' is defined as the lateral separation between the points on any projected plane parallel to the cascade axis, beyond which the projected particle number density is less than 1·5 mm^{-1}. The Monte Carlo simulations have been generated for various energies in the range 10–5000 GeV and also for some pure electromagnetic cascades of comparable energy.

The average growth curves for hadrons of different primary energy are shown in figure 1 for the three models. Due to the rather large computing time required for generating cascades of energy greater than about 500 GeV (~3 hours per 1000 GeV

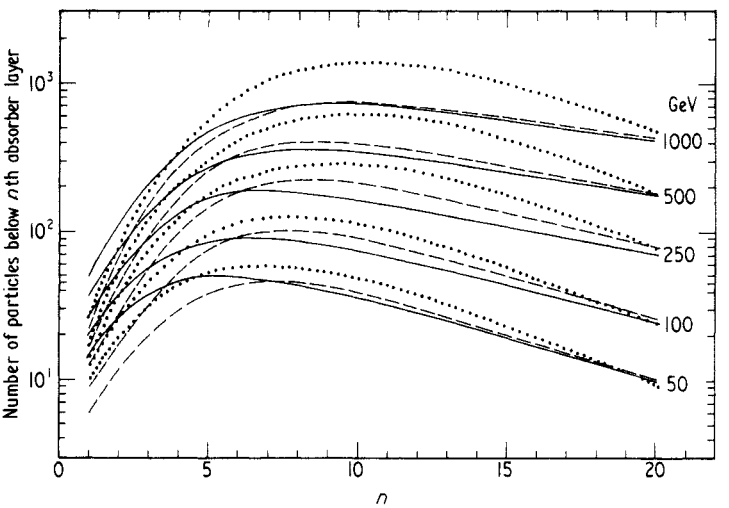

Figure 1. The average number of tracks below plates for hadron-initiated cascades of different energy according to models A (broken line), B (full line) and C (dotted line). Each plate corresponds to one radiation length. It is seen that the model C gives the fastest rise and absorption.

cascade), the typical number of cascades generated for such energies is only 10 for each model. The average cascade curves obtained are therefore not very smooth since the fluctuations in individual cases are considerable. However, in figure 1, smooth curves drawn through the available points are shown. An interesting feature seen in figure 1 is the variation of the rate of development and absorption in the different models. As expected, in the early stages of development, due to the assumed smaller multiplicity in the hadron interactions, the model A gives a slower rate of development for the cascades. The later stages are similar in both models A and B implying that the multiplicity in hadron interactions does not affect the number of tracks in the later stages and therefore the integrated track length is not substantially different for models A and B especially at high energies. The model C, on the other hand, gives the fastest rate of growth and absorption for the cascades.

The extent of fluctuations in the number of particles at different stages of the cascade can be seen from figure 2. For cascades of 100 GeV the fluctuations tend to be somewhat larger if the hadron interactions are assumed to be partially elastic (model B). At higher energies fluctuations are considerably reduced.

The average cascade width after any absorber layer increases logarithmically with the number of particles below the layer as can be seen from figure 3. While the number of tracks decreases after the cascade maximum, in some cases depending upon the number of absorber layers after which the maximum is reached, the cascade width continues to increase and then falls off rapidly. This is due to the broadening of the lateral distribution and the particular definition of cascade width which we adopted. Model A is expected to give very similar cascade widths for energies above about 500 GeV beyond about the fifth layer. The relation between the number of particles below the nth absorber layer and the hadron energy for the two models is given in figure 4. Typical fluctuations in the cascade widths at different absorber layers obtained from the simulations for 1000 GeV cascades are shown in figure 5. The model C clearly gives broader cascades compared to the model B. The standard deviation in the width distribution is about 20% for widths after the six absorber layer at all energies and about 30% for widths after the fifteenth layer, for cascades greater than about 500 GeV.

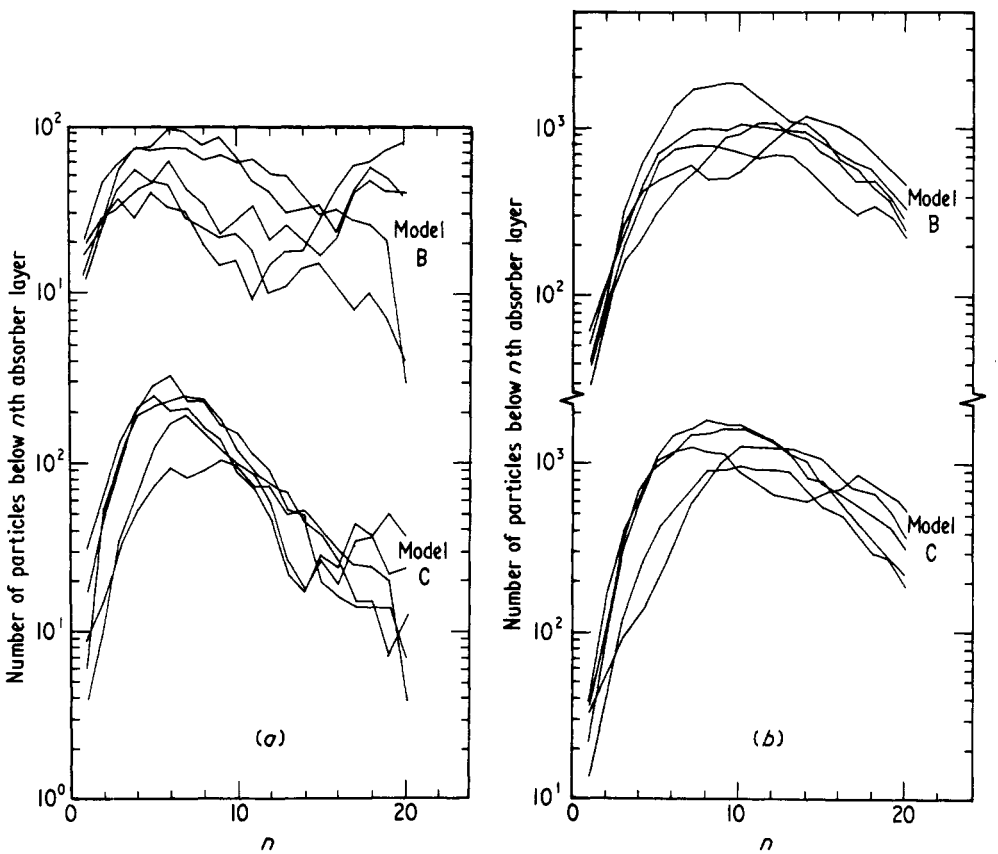

Figure 2. Several instances of Monte Carlo simulations for (*a*) 100 GeV and (*b*) 1000 GeV hadron cascades giving the relation between the number of particles and the plate number. Each cascade is assumed to start at plate 1.

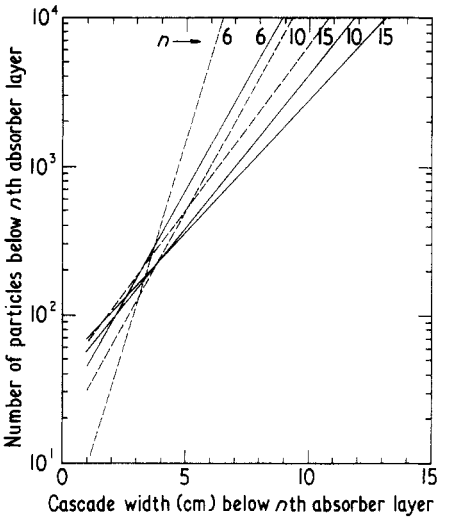

Figure 3. Typical curves giving the relation between the projected cascade widths and the number of particles corresponding to different plate numbers. The same cascade width corresponds to different number of particles after different plate numbers in the same model. The definition of projected width is given in the text. Full line model B, broken line model C.

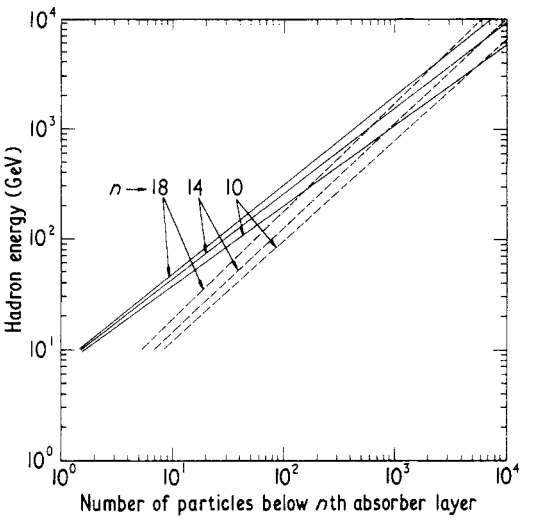

Figure 4. Typical curves giving the relation between the hadron energy and the number of particles after different absorber layers according to models B (full line) and C (broken line).

3. Methods of cascade energy determination in the multiplate cloud chamber

3.1. Track length integral by counting individual tracks

As mentioned earlier, it is possible to count the number of tracks below practically all the plates in the case of cascades of energy less than about 200 GeV. The calculations give the relation between the particle number integral up to the nth absorber layer and

the primary hadron energy, similar to that shown in figure 6 for two typical values of n and for the models B and C. For comparison the curves for γ ray cascades are also given in the same figure. The fluctuations in the number integral for different values of n

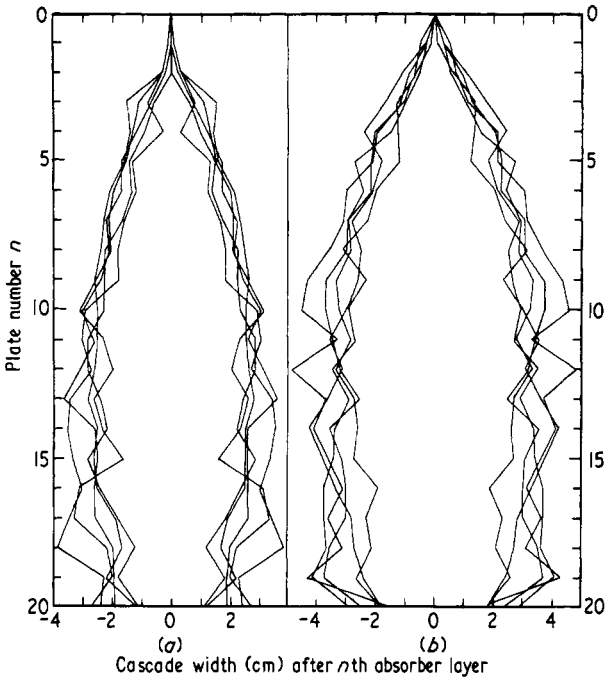

Figure 5. Typical cascades showing the relation between the projected cascade width and plate number for 1000 GeV cascades for (*a*) model B and (*b*) model C to illustrate the extent of fluctuations in cascade widths.

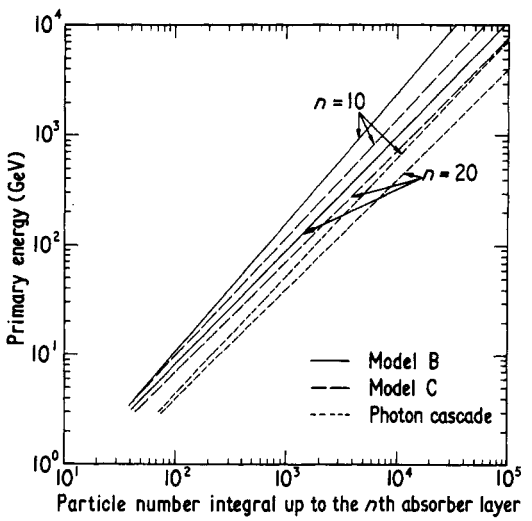

Figure 6. Typical cascades giving the relation between the hadron energy and the particle number integral corresponding to different stages of the cascade. The curves are given for the models B and C and also for pure electromagnetic cascades corresponding to two different stages, n = 10 rl and n = 20 rl.

and for models B and C are shown in figure 7 along with similar fluctuations for photon cascades. It is interesting to see that while for the photon cascades the number integral obtained just up to the tenth absorber layer has a standard deviation of only about 10%, for hadron cascades it is as high as 40%, but independent of the interaction model. However, if all the 20 radiation lengths in the multiplate cloud chamber are available for counting the number of tracks, the effect of fluctuations is considerably reduced.

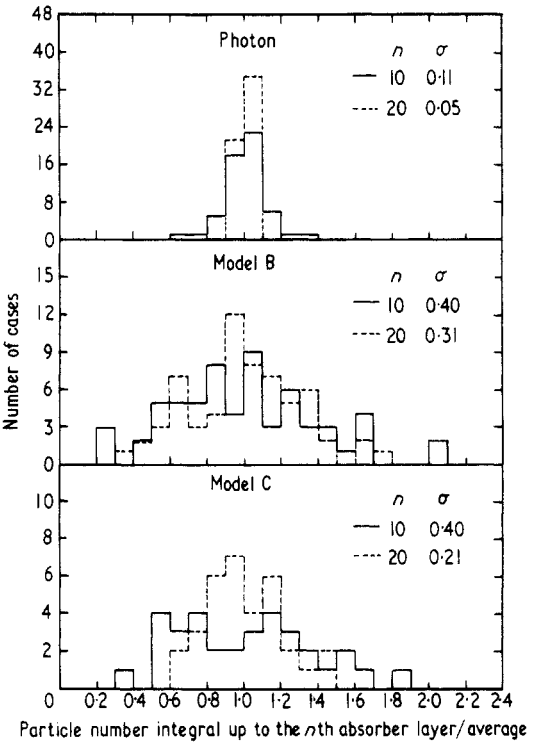

Figure 7. Histograms for cascades of energy less than 200 GeV showing the extent of fluctuations in the particle number integral up to the tenth and twentieth layers.

It is seen from figure 6 that for the number integral up to the tenth absorber layer, the energies given by model B are about 30% higher than those given by model C for hadrons of energy about 100 GeV. This difference is reduced if a larger number of absorber layers are available for obtaining the particle number integral. However, as will be evident from § 4, the observed cascades in the chamber fit the models A and B better than model C for energies up to a few hundred GeV. Consequently the energy uncertainty is considerably reduced.

A typical cascade observed in the cloud chamber where the track length is obtained by counting of tracks, is shown in figure 8 (plate) and the hadron energy determined from the track length integral up to the fifteenth absorber layer for this cascade is 200 GeV.

3.2. Track length integral by measuring cascade widths

For cascades of energies greater than about 200 GeV the cascade widths can be measured generally from about the third absorber layer and the corresponding particle number

below each plate can be obtained using the relations of the type shown in figure 3 for models B and C. (Models A and B are expected to give similar width to track number relations after about the fifth absorber layer where the measurements matter most for the energy estimate.) Thus measurement of widths allows the determination of the particle number integral even for higher energy cascades, using the results of the Monte Carlo simulations. The primary hadron energy is then obtained from the integral track length. However, since the width is logarithmically related to the particle number the fluctuations in the measured widths have a much larger effect on the particle number integral. Therefore the distribution of the number integral obtained indirectly through cascade widths is somewhat broader compared to direct counting of tracks. The values of the standard deviation for this integral up to the tenth and the twentieth absorber layers are 49% and 34% respectively, as shown in figure 9. Though this error may seem large compared to the error of less than 30% in the energy measurement obtainable by the use of ionization calorimeters, it is still quite satisfactory considering the advantages gained by having a visual detector like the cloud chamber. If the energy is estimated directly from the integral track length as in the case of an ionization calorimeter, the accuracy in the estimate of the energy is much better as can be seen from figure 10. The energy estimated by the cascade width method is not too sensitive to the interaction model as will be shown later. A typical *rapidly attenuating* cascade whose energy has been estimated as 750 GeV using this method is shown in figure 11 (plate) and a typical cascade having an *elongated structure* whose energy has been estimated as 2400 GeV is shown in figure 12 (plate).

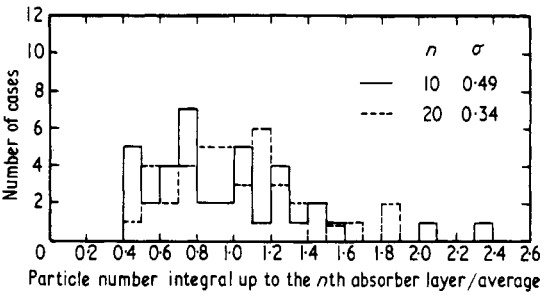

Figure 9. Histogram showing the extent of fluctuations in the particle number integral (model B) for cascades of energy $\gtrsim 200$ GeV where the method of cascade widths is used. The standard deviations of the distributions are 0·49 and 0·34 for 10 and 20 rl respectively.

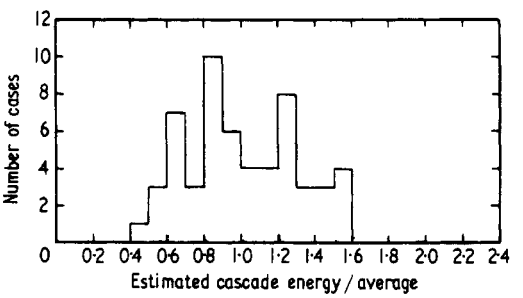

Figure 10. Histogram showing the extent of uncertainty in the energy estimate if the track length integral could be evaluated by a total ionization calorimeter method. The standard deviation of the distribution is 0·30.

3.3. Energy estimation for a hadron cascade associated with considerable air shower background

The two methods of energy estimation discussed above are applicable in practice only when the hadron cascade is isolated and there is no significant track background in the cloud chamber to hamper the measurements in the early part of the cascades. However, the high energy hadrons associated with air showers due to their nearness to the shower axis, frequently arrive at the chamber accompanied by a large number of electrons as well as low energy hadrons. In such cases the shielding above the chamber is not very effective and it becomes difficult to measure the particle number or the cascade widths with sufficient accuracy in the early stages of the cascades. We find that the method of simulated cascades can still be adopted for energy estimation using the cascade widths measured in the tail regions provided the point of initiation of the cascade can be made out clearly. Instead of using the integral track length, the cascade widths or track counts measured at several depths in the tail region are used to obtain the probable energy of the cascade through the relations of the type shown in figure 4. The average of the energies obtained from particle numbers corresponding to several depths then gives an estimate of the primary hadron energy. However the energy estimated using this method is to some extent model sensitive. The fact that the cascades do fit particular models better in particular energy regions tends to reduce the effect of the interaction model on the estimated energy. If large numbers of measurements near cascade maxima are possible it is estimated that the energy determined by this method is accurate to within about 40–50 %. Very near the tail of the cascades the fluctuations tend to be high. The fluctuations become very large beyond the fourteenth plate for 100 GeV cascades and beyond the seventeenth or eighteenth plate for cascades of 250 GeV. Thus such regions of large fluctuations have to be avoided to maintain good accuracy in the energy determination.

Figure 13 (plate) is an example of an event in which the energy of the hadron has to be determined in the presence of a large number of air shower particles. The starting point of the higher energy cascade can be seen in the original negative when directly viewed against light. It is however not possible to make any measurements in the earlier part of the cascade. By measuring the cascade widths in the tail region the energy of this cascade has been estimated to be about 450 GeV.

4. Comparison of experimental and theoretical cascades: characteristics of high energy collisions

4.1. Hadrons of energy 25–200 GeV

In this energy range, as pointed out earlier, it is feasible to obtain the track length by counting the number of tracks below the various plates. We have seen that for cascades of less than 200 GeV the energy evaluation of the cascades from the integral track length is relatively insensitive to the models of nuclear interaction tried out, provided a minimum potential track length corresponding to about 10 radiation lengths is available (figure 6). The model dependence of the detailed profiles of the cascade development curves can be judged from figure 1. In order to see what conclusions can be drawn regarding the validity of the different models, we have in figure 14, compared the experimentally obtained cascade curves with the calculated ones drawn for the three different models. For this purpose, the experimental cascades have been classfied into three energy groups: 25–50, 50–100 and 100–200 GeV and the corresponding weighted

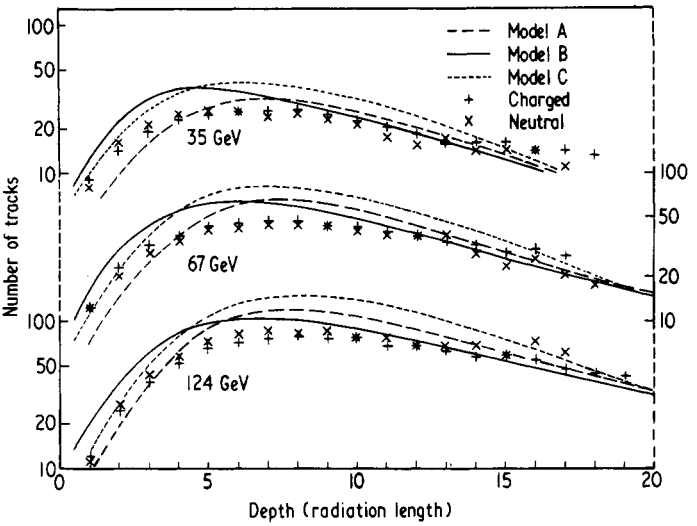

Figure 14. Comparison between the profiles of the experimental and calculated cascade curves giving the relation between the number of tracks and radiation length. The experimental points correspond to the weighted mean averages of cascades in three energy ranges (25–50, 50–100 and 100–200 GeV). The theoretical curves have been drawn for the weighted mean average energies of 35, 67 and 124 GeV. The experimental points for neutral (×) and charged (+) hadron cascades are shown separately.

average numbers of tracks have been obtained and compared with the calculated curves for average energies of 35, 67 and 126 GeV respectively. The data corresponding to charged and neutral hadrons have been plotted separately. It can be seen from figure 14 that within the energy range 25–200 GeV there is no variation in the behaviour of the cascade curves with energy. The experimentally obtained cascade curves appear, in general, to be flatter than the calculated ones after the cascade maxima. The agreement is closest with respect to the models A and B and the disparity is most with respect to the model C. The very important feature to be noted is that there is no difference in the cascade curves of charged and neutral hadrons. In this energy range one knows experimentally, from the cloud chamber results (Sreekantan 1971), that in showers of size 5×10^4 to 5×10^6 particles at 800 g cm^{-2}, the charged to neutral ratio of hadrons is about three and consequently one expects that about two thirds of the charged hadrons would be pions. If pion interactions are completely inelastic, then one would expect the cascade curves of charged particles in figure 14 to be closer to model C than to models A and B. Since this is not the case, the pion collisions may not be completely inelastic and probably are similar to nucleon collisions in this energy range†. In this connection, it is interesting to point out that similar conclusions can be drawn from the experimental results of Orlova and Tretyakova (1971) who have studied the most energetic pions emerging from 60 GeV pion interactions at the Serpukov accelerator.

4.2. Hadrons of energy 200–500 GeV

In figure 15, a comparison is made between the experimental and calculated curves for hadrons in the energy range 200–500 GeV. The energy range is divided into two groups,

† It should be pointed out that these conclusions will remain valid even if there is a systematic error as high as 30% in the actual energy estimates.

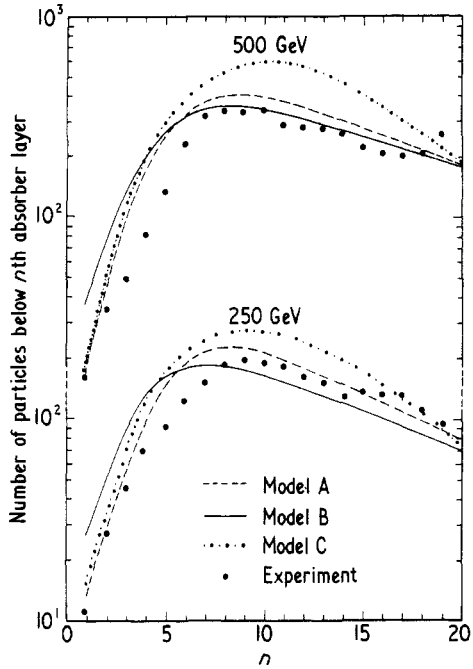

Figure 15. Comparison of the experimental and calculated profiles of track number for cascades in the energy range 200–500 GeV. The experimental cascades are divided into two groups, one having a weighted mean energy of 230 GeV and the second 430 GeV. The calculated curves have been drawn for 250 and 500 GeV.

the first having an average energy of 230 GeV and the second of 430 GeV. The experimental points have been obtained by direct track counts or from the cascade widths by using relations of the type given in figure 3. The errors on the experimental points are small. The calculated curves for the three models have been drawn for energies of 250 GeV and 500 GeV respectively, for comparison. It is seen that in the growth part of the cascades the experimental ones have a slower rate while the decay parts are consistent with models A and B and disagree with model C. The slower rise observed experimentally especially at energies of approximately 500 GeV suggests that the multiplicity of secondary particles (effective in cascade growth) assumed in the models is too high at such energies.

4.3. Hadrons of energy greater than 10^{12} eV

In figure 16, the average features of the cascade width curves for hadron interactions in the energy range 1–10 TeV are compared with the calculated curves based on models B and C. Also shown in the same figure is a comparison between the experimental average cascade width curve and the calculated ones for an average energy of 460 GeV. Sometimes, in these cases, a direct track count is possible during the early stages of the cascade. At such energies in regions past the cascade maxima and especially near the tail of the cascades, the width as defined by us, is subject to large fluctuations due to secondary contributions; width measurements become critical and possibly biased. Thus in some cases a direct track count in such regions is more meaningful and feasible. Hence at

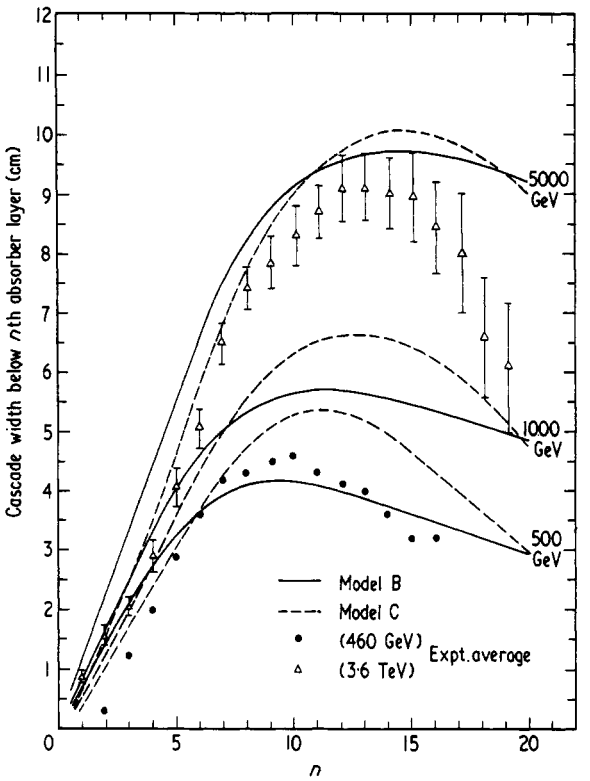

Figure 16. Comparison of the experimental and calculated profiles of cascade width for cascades in the TeV region. The experimental points are the weighted averages for 13 cascades in the energy range 1–10 TeV. The faster rate of absorption of the cascade even compared to model C is apparent. The bottom curves for cascades of energy 500 GeV are shown to illustrate that at these energies the cascade width drops off very fast after the maxima due to the lateral spread of particles. In such cases it becomes feasible to count the number of tracks and use them for interpretation.

these energies the conclusions must be based on the final track number attenuation (as in figure 15) rather than on the rate of attenuation of the cascade widths. The experimental points in the TeV region show an absorption feature after the cascade maximum which is closer to that given by model C than model B. In fact, there appears to be a tendency for the experimental points to show a slightly faster absorption than even that given by model C. This is extremely interesting and important since the cascades of lower energy, as we saw in the previous paragraph, show a clear preference to model A (or B), rather than C. This effect cannot be explained by any systematic errors in measurement.

As seen in the last section, model B assumes too high a multiplicity and this is also reflected in the growth of the width curves in figure 16. This does not affect the energy estimation since firstly model A has been used for conversion of integral track length to primary energy and secondly the contribution to the track length integral from the initial region of the cascade is small.

The charged to neutral ratio for hadrons of energy greater than 200 GeV associated with air showers in the size range 5×10^4 to 5×10^6 particles at 800 g cm^{-2} obtained with the same cloud chamber is about one which means that at these energies pions are negligible compared to nucleons. Therefore the above result concerning fast absorption

cannot be attributed to the increase of pions among the hadrons, even if we make the assumption that the pion induced cascades have this fast absorption feature. In order to reproduce the fast absorption of the cascades, it is necessary therefore for the nucleon interactions in the TeV energy range to be not only highly inelastic but also give rise to a secondary particle spectrum which is considerably softer than at lower energies. Such a model is consistent with the increase of $\overline{K}_\gamma$ at high energies observed in the hadron–Pb interactions by Nam *et al* (1971).

We would like to emphasize however that the fast absorption in the TeV cascades is only an average picture for we do have cascades which have elongated tube-like structures that do not show such fast absorption.

Since the TeV cascades show a closer fit to the model C it would be more appropriate to use this model for the evaluation of the cascade energies in this region. However, it has been found that even if the energy estimate is made using the model B instead of model C *and the method of cascade widths is used*, at energies of about 10^{12} eV the energy is overestimated by only 15% and at 5×10^{12} eV underestimated by about 8%. Thus our method of energy estimation is applicable to the entire energy region from 25 GeV to several TeV using the same model for calibrations.

5. Conclusions

It is possible to determine the energy of hadrons up to 10^{13} eV with an accuracy better than 50% in a large multiplate cloud chamber, using for energy calibration Monte Carlo simulations of track lengths and cascade widths corresponding to the various stages of development and absorption of these cascades in the cloud chamber. The energy estimates are reasonably independent of the details of the characteristics of interactions.

The development and absorption of the cascades due to pions and nucleons are very similar at energies below 200 GeV and a comparison with different models of interactions shows that the collisions of both pions and nucleons are only partially inelastic at these energies.

Hadron cascades in the energy range 1–10 TeV associated with air showers show a relatively faster absorption after the cascade maxima. For the explanation of this feature it is necessary to assume an increase in the inelasticity and multiplicity† in TeV collisions resulting in the production of a large number of secondaries of relatively low energy. The 'Gammaization' process in nucleon collisions at $E > 10^{13}$ eV proposed by Nikolsky (1967) to explain several features of air showers could also account for the type of behaviour observed in the present experiment, if a similar process becomes operative even at energies of a few TeV.

It is important to note that in the present experiment we are dealing with nucleon–iron nucleus collisions. It is conceivable that in such collisions the effects of collective interactions of nucleons bound in the iron nucleus might become dominant at TeV energies. It may be pointed out that recently Grigorov *et al* (1971) have highlighted the importance of collective interactions in the collisions of heavy primaries of several TeV/nucleon with the nucleons in air nuclei. Thus, it is necessary to see whether collective interactions in collisions of nucleons on the iron nucleus could lead to either of the possibilities considered to explain the observed faster absorption.

† As seen from the cascade growth at such energies actual multiplicity is still smaller than that given by model B.

Acknowledgments

It is a pleasure to thank Dr B K Chatterjee and Dr G T Murthy for many fruitful discussions. We wish to express our thanks to N V Gopalakrishnan for help in the analysis of the experimental data and to A R Apte and S G Khairatkar for assistance in the operation of the cloud chamber and the EAS array. Lastly, we are indebted to Dr K Sivaprasad for making useful suggestions during the final stage of this work.

Appendix 1. Hadron interactions

Three different models of interactions A, B and C have been constructed and used in the calculations. All the interactions are treated in the laboratory system itself and the energetic particles like recoil nucleons going backwards in the centre of mass system are ignored due to their rather small energy in the laboratory system.

(i) The interaction mean free paths for nucleon–iron nucleus and pion–iron nucleus collisions have been taken as 130 and 140 g cm^{-2} respectively and have been assumed to be independent of hadron energy as suggested by various experiments (eg Bussian *et al* 1971, Bashindjhagyan *et al* 1971).

(ii) The nucleon interactions have been considered to be partially elastic in the models A and B where it is assumed that after the interaction the nucleon emerges with 80 % of its original energy either in an excited state (probability 0·7) or in the normal state (probability 0·3). The excited state decays into a nucleon and one to three pions depending on the energy of the interacting nucleon. These features about the isobar formation are based on the phenomenological model suggested by Pal and Peters (1964) to explain various observed cosmic ray phenomena. However, in the model C no such isobar formation is considered since the hadron interactions are assumed to be completely inelastic.

The pion interactions have been assumed to be completely inelastic in model A and partially elastic (average inelasticity = 0·6) in model B. While in model A or C no fluctuation in inelasticity has been considered, a distribution of the form of sin θ around the average ($\theta = \pi/2$) has been taken between the values 0·2 and 1, in the model B.

(iii) The multiplicity in an interaction of a nucleon of energy E (GeV) is assumed $\propto E^{1/2}$ in models A and B and $\propto E^{1/4}$ in model C. To consider the effect of higher multiplicity expected due to the intranuclear cascade in an iron nucleus, the effective multiplicity in model B is assumed to be $1{\cdot}0E^{1/2}$ compared to only $0{\cdot}34E^{1/2}$ in model A, excluding the isobar decay products. This assumption in model B is again an extreme assumption and has been made to distinguish the difference in cascade features due to different multiplicities. The multiplicity in model C is taken as $2{\cdot}7E^{1/4}$. The fluctuations in multiplicity in individual interactions have been considered either in the form of a uniform distribution between the values $0{\cdot}5\bar{n}$ and $1{\cdot}5\bar{n}$ (models A and C) or in the form of a sin $\theta(\theta = \pi/2$ at $n = \bar{n})$ distribution between the values 0 and $2\bar{n}$ (model B), where $\bar{n}$ is the average multiplicity. The available experimental data on the multiplicity–energy relationship, at least up to energies of about 1000 GeV are consistent with the assumptions of either of the models A or C (see, for example, Grieder 1971).

In the case of pion interactions the average effective multiplicities assumed for the models A, B and C are $1{\cdot}5E^{1/4}$, $3{\cdot}7E^{1/4}$ and $2{\cdot}7E^{1/4}$ respectively. Similar to nucleon interactions the multiplicity is assumed to be rather high in model B for the reasons mentioned above. Fluctuations in multiplicity similar to those for nucleon interactions have also been considered in pion interactions.

(iv) The energy and transverse momentum distributions for fireball particles have been assumed to be of the forms suggested by Cocconi *et al* (1962) (see also Cocconi 1971) on the basis of the available experimental data. Thus $n(E)\,dE \propto e^{-aE}\,dE$ and $n(p_t)\,dp_t \propto p_t \exp(-p_t/p_0)\,dp_t$ where a is a constant determined for each interaction from the energy conservation condition and p_0 equals 0·18 GeV/c. The energies and momenta of the isobar products are determined kinematically.

(v) All the secondary particles produced are assumed to be only pions, the neutral ones being one third of all. Though kaons and baryons are known to be produced, the kaons ($\sim$5–10%) have been ignored due to their indistinguishable interaction features compared to pions and small decay probability in the 1·5 m high absorber assembly. The baryons are not considered since they are known to be only about 1% of the produced particles in interactions of about 20 GeV (Turkot 1968) and increase to about 15% only at very high energies of about 10^4 GeV (Tonwar *et al* 1971).

(vi) The iron nucleus disintegration is assumed to take away 800 MeV from the interacting energy (Murzin 1967). The slow particles and the nuclear fragments resulting from the disintegration rarely come out of the absorber layer due to their high rate of energy loss and have not been considered individually. They do not affect any of the measured cascade parameters observed in the cloud chamber in any significant manner.

Appendix 2. Electromagnetic processes

Using the standard formulae for the various electromagnetic processes discussed by Rossi (1952) the probability of a photon of energy E (GeV) materializing in 1 g cm^{-2} of absorber (iron) and giving an electron of energy between 0 and E' is

$$W_{pp}(E, E') = 0{\cdot}0703\left(\frac{E'}{E}\right) - 0{\cdot}0478\left(\frac{E'}{E}\right)^2 + 0{\cdot}0319\left(\frac{E'}{E}\right)^3.$$

Thus the total probability ($E' = E$) per g cm^{-2} is 0·0544 and the pair production mean free path in iron (λ_{pp}) is 18·4 g cm^{-2}. These relations are applicable only for energies larger than the critical energy (23 MeV) in the iron medium where complete screening can be assumed. In order to simplify the calculations complete screening is assumed for electron or photon energies greater than 23 MeV and no screening for lower energies. The pair production mean free path for photon energies smaller than 23 MeV is taken as

$$\lambda_{pp} = \frac{59{\cdot}2}{(7/9)\ln(2E/m_e) - 2{\cdot}02}$$

where m_e is the electron mass (GeV). The Compton scattering mean free path λ_{Cs} in iron is obtained similarly as

$$\lambda_{Cs} = \frac{2{\cdot}86 \times 10^4 E}{\ln(2E/m_e) + 0{\cdot}5}$$

from the integral probability distribution

$$W_{Cs}(E, E') = \frac{0{\cdot}069 m_e}{E}\left\{\ln\left(\frac{E'}{E}\right) + \frac{1}{2}\left(\frac{E'}{E}\right)^2 + \ln\left(\frac{2E}{m_e}\right) - \frac{1}{2}\left(\frac{m_e}{2E}\right)^2\right\}$$

where E' is the energy of the scattered photon. Using the random number subroutine and the mean free paths evaluated as above the process occurring first for a particular

photon and its location in the absorber are determined. The energies of the resulting electrons and photons are determined from the probability distributions through iterative procedures.

The bremsstrahlung radiation process of electrons has been divided into two parts—emission of photons of energies less than 1 MeV and of photons of energies greater than 1 MeV. The former is treated as a continuous process and the energy loss of the electron due to the emission of these low energy photons is taken into account. E_{rad} (MeV/g cm^{-2}) is given by the equation

$$E_{rad} = E\left\{0{\cdot}0956\left(\frac{E_{min}}{E}\right) - 0{\cdot}0478\left(\frac{E_{min}}{E}\right)^2 + 0{\cdot}0237\left(\frac{E_{min}}{E}\right)^3\right\}.$$

In the calculations E_{min} has been taken as 1 MeV. This value for E_{rad} is applicable only for electrons of energies greater than 23 MeV; the energy loss for lower energy electrons is given by

$$E'_{rad} = \frac{E_{rad}}{f_{rad}} \qquad f_{rad} = \ln\frac{\{(2E/m_e) - 0{\cdot}33\}}{4{\cdot}21}.$$

For electrons of energies greater than 1 MeV the mean free path for photon emission is calculated using the integral probability for the process given by

$$\Phi_{rad} = 0{\cdot}0956\left(\frac{E_{min}}{E}\right) - 0{\cdot}0956\ln\left(\frac{E_{min}}{E}\right) - 0{\cdot}0352\left(\frac{E_{min}}{E}\right)^2 - 0{\cdot}0604.$$

Again, for electron energies less than 23 MeV the correction for the absence of screening has been applied. The energy of the emitted photon at the point determined by using Φ_{rad} is obtained from the probability distribution for the process, W_{rad}†.

The collision loss for the electrons has been considered as a continuous process and the electron is assumed to lose 1·6 MeV/g cm^{-2} of its travel. The scattering suffered by the electrons has been considered in great detail and the absorber has been divided into thin strips to calculate the scattering angle for low energy electrons. The thickness of these strips is taken as $5 \times 10^{-4}\,E$ radiation lengths where E is the electron energy in MeV. Due to the thinness of these strips the scattering angle in any strip is small and the small angle approximation used in deriving the scattering relations remains valid. The Moliere theory of multiple scattering given by Bethe (1953) gives the differential probability for an electron to be scattered by an angle between θ and $\theta + d\theta$ in travelling a medium of thickness t radiation lengths as

$$f(\theta)\,d\theta = K\left(\frac{\sin\theta}{\theta}\right)^{1/2}\phi\left(f^0(\phi) + \frac{1}{B(t)}f^1(\phi)\right)d\theta.$$

The various quantities appearing in this expression are defined as

$$\phi = 0{\cdot}19\theta E(tB)^{-1/2}$$

$$B - \ln B = 10{\cdot}795 + \ln t$$

$$f^0(\phi) = 2\exp(-\phi^2)$$

$$f^1(\phi) = 2\exp(-\phi^2)(\phi^2 - 1)\left(\int_{-\infty}^{\phi^2}\frac{e^y}{y}\,dy - \ln(\phi)^2\right) - 2\{1 - 2\exp(-\phi^2)\}.$$

† W_{rad} is obtained by replacing E_{min} by E' in Φ_{rad}.

K is a normalization constant and has been determined numerically by integrating $f(\theta)$. For electron energies greater than 1 GeV the scattering has been considered through the calculation of the mean square angle θ(rad)

$$\theta = \frac{42t^{1/2}}{\{2E-(1/2E)\}^{1/2}}.$$

Many of the relations used above were calculated for various values of the variables and stored in the computer memory to save on the computation time. Though for all lower energy cascades the cut-off energy for electrons or photons has been taken as 1 MeV, for higher energy cascades this has been sometimes taken as 10 MeV to reduce the computation time. However, in such cases a few cascades were always generated using 1 MeV as the cut off to provide the corresponding scaling factors.

References

Bashindjhagyan G L, Murzin V S, Sarycheva L I and Sinyov N B 1971 *Proc. 12th Int. Conf. Cosmic Rays, Hobart* 1971 vol 6 (Hobart: Univ. of Tasmania) pp 2211–28

Bethe H A 1953 *Phys. Rev.* **89** 1256–66

Bussian A E *et al* 1971 *Proc. 12th Int. Conf. Cosmic Rays, Hobart* 1971 vol 3 (Hobart: Univ. of Tasmania) pp 1194–9

Cocconi G 1971 *Nucl. Phys.* B **28** 341–8

Cocconi G, Koester L J and Perkins D H 1962 *UCRL Report no* UCRL-10022

Grieder P K F 1971 *Proc. 12th Int. Conf. Cosmic Rays, Hobart* 1971 vol 3 (Hobart: Univ. of Tasmania) pp 1265–70

Grigorov N L *et al* 1971 *Proc. 12th Int. Conf. Cosmic Rays, Hobart* 1971 vol 6 (Hobart: Univ. of Tasmania) pp 2229–33

Murzin V S 1967 *Progress in Elementary Particle and Cosmic Ray Physics* vol 9 eds J G Wilson and S A Wouthuysen (Amsterdam: North Holland) pp 247–303

Nam R A *et al* 1971 *Proc. 12th Int. Conf. Cosmic Rays, Hobart* 1971 vol 6 (Hobart: Univ. of Tasmania) pp 2259–72

Nikolsky S I 1967 *Sov. Phys.–JETP* **24** 535–45

Orlova G I and Tretyakova M I 1971 *Proc. 12th Int. Conf. Cosmic Rays, Hobart* 1971 vol 6 (Hobart: Univ. of Tasmania) pp 2297–306

Pal Y and Peters B 1964 *K. danske Vidensk. Selsk., Math.–fys. Meddr* **33** no 15

Rossi B 1952 *High Energy Particles* (Englewood Cliffs, NJ: Prentice-Hall)

Sreekantan B V 1971 *Proc. 12th Int. Conf. Cosmic Rays, Hobart* 1971 (Hobart: Univ. of Tasmania) *TIFR Preprint no* CR-EAS-5

Tonwar S C, Naranan S and Sreekantan B V 1971 *Lett. Nuovo Cim.* **1** 531–7

Turkot F 1968 *Proc. 2nd Topical Conf. High Energy Collisions of Hadrons, CERN* 1968 vol 1 (Geneva: CERN) pp 316–44

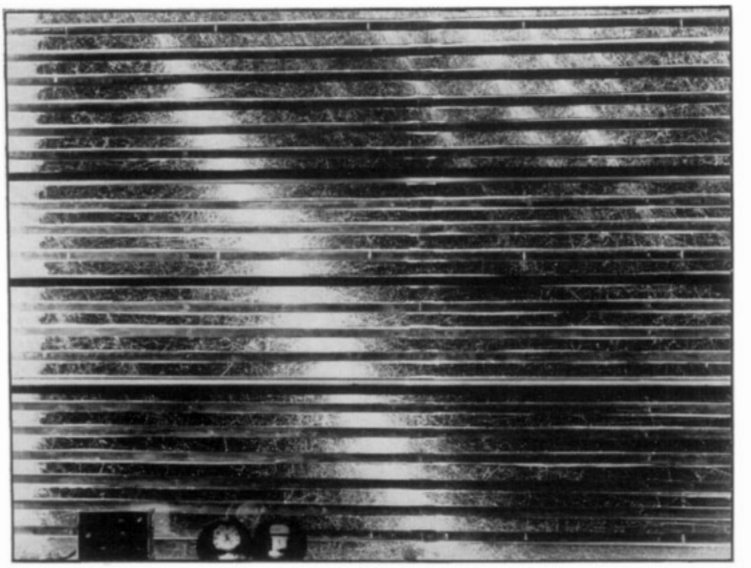

Figure 12. A cascade having an elongated tube-like structure which is not completely absorbed even after 20 radiation lengths. The estimated energy is 2·4 TeV.

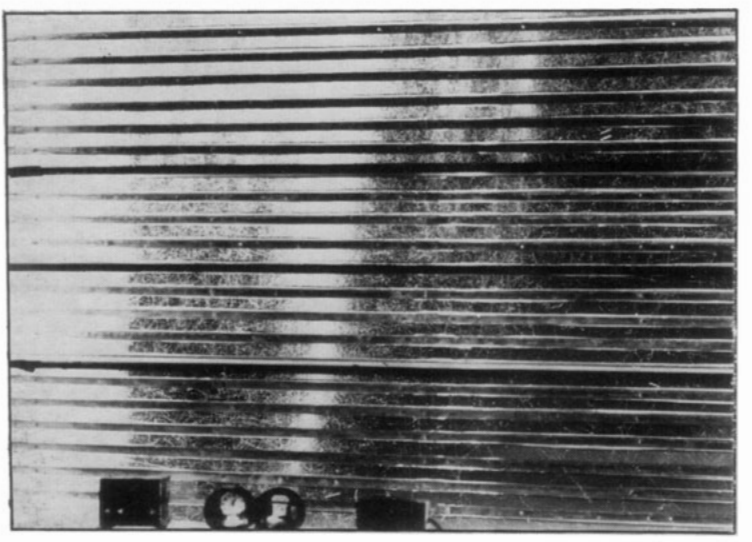

Figure 13. A cascade accompanied by soft particles and low energy hadrons. The point of initiation of the cascade can be recognized by examining the negative against strong light. The energy estimate is made by the method of cascade widths using the tail region. Distortion observed in the lower part is due to turbulence which however does not affect the energy measurement. The estimated energy of the cascade is 450 GeV.

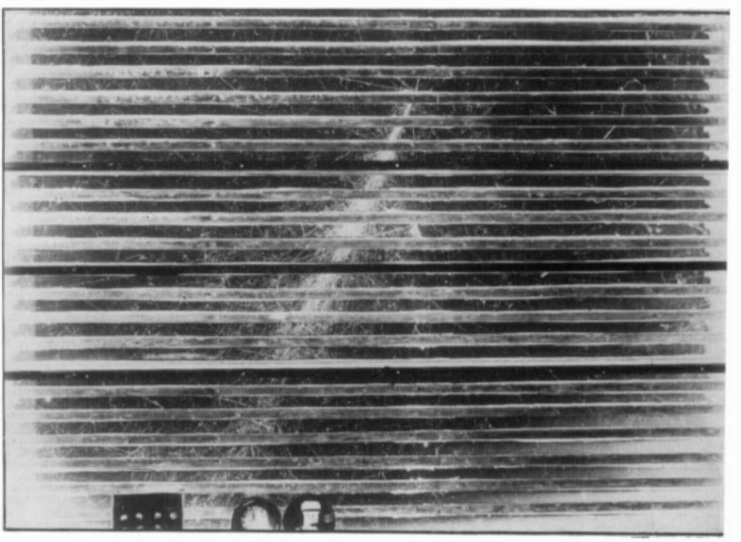

Figure 8. A typical cascade which starts in the fourth plate of the chamber. It is possible to count the number of tracks at all stages of development and absorption and obtain the integral track length. The energy of the cascade is 200 GeV.

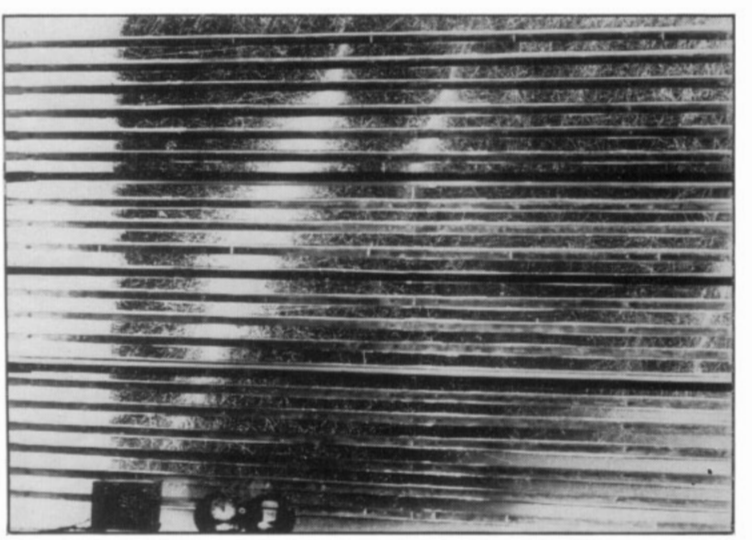

Figure 11. A cascade which develops from the first plate of the chamber and shows a rapid absorption after the maxima. The method of cascade widths has been used for energy estimation which is 750 GeV.